Granular Matter (2011) 13:29–37
DOI 10.1007/s10035-010-0220-9

Heat transport in granular materials during cyclic fluid flow

T. S. Yun · B. Dumas · J. C. Santamarina

Received: 10 September 2008 / Published online: 1 October 2010

Abstract Heat transfer takes place between grains and the fluids that saturate the pore space in granular materials, when the fluid is static or moving. This study explores effective heat transport in granular materials during cyclic fluid flow. Controlled particle-scale experiments, complementary analyses and numerical simulations help us identify the governing variables and ensuing time scales. We show that fluid-grain heat transfer leads to effective heat transport along the granular medium during cyclic fluid flow. At the macro-scale, the process resembles diffusion where the effective diffusion coefficient is proportional to the square of the fluid invasion length in each cycle and inversely proportional to the cycle period. Both experimental and numerical results confirm improved heat transfer by cyclic fluid flow over thermal diffusion under hydrostatic conditions. The formulation can be used to identify optimal operation conditions for maximum transport.

Keywords Heat transfer · Diffusion · Cyclic flow · Granular material

T. S. Yun (✉)
Department of Civil and Environmental Engineering,
Yonsei University, 262 Seognsan-ro, Seodaemun-gu,
Seoul 120-749, Korea
e-mail: taesup@yonsei.ac.kr

B. Dumas
Department of Civil and Environmental Engineering,
Lehigh University, 13 East Packer Avenue, Bethlehem,
PA 18015, USA
e-mail: bcd209@lehigh.edu

J. C. Santamarina
School of Civil and Environmental Engineering, Georgia Institute
of Technology, Atlanta, GA 30332-0355, USA
e-mail: jcs@gatech.edu

List of symbols

t_{cy}	Cycle period (s)
t_{ch}	Characteristic time (s)
r_p	Particle radius (s)
k	Thermal conductivity ($\mathrm{W\,m^{-1}\,{}^{\circ}C^{-1}}$)
c	Heat capacity ($\mathrm{kJ\,kg^{-1}\,{}^{\circ}C^{-1}}$)
ρ	Mass density ($\mathrm{kg\,m^{-3}}$)
T_{hw}	Temperature of hot water bath (°C)
T_{cw}	Temperature of cold water bath (°C)
T_p	Temperature of particle (°C)
Q	Thermal energy (J)
q	Heat transfer rate (W)
α	Proportional thermal energy in the fluid phase
Ψ	Heat loss coefficient ($\mathrm{W\,{}^{\circ}C^{-1}}$)
M	Discretization modulus—numerical solution of the diffusion equation
D	Thermal diffusivity ($\mathrm{m^2\,s^{-1}}$)

1 Introduction

The thermal conductivity k of granular materials depends on the material that makes the grains, the fluid that fills the pore space and intergranular contact conditions. The thermal interaction between phases and fabric leads to the following ordered sequence of thermal conductivity values in the case of sediments, i.e., granular materials made of mineral grains: $k_{mineral} > k_{saturated\_granular} > k_{water} > k_{dry\_graunlar} > k_{air}$ [1–3]. The contact models to evaluate the heat propagation in particulate materials under static and dynamic condition often highlight the significance of intergranular state [4,5]. Despite its inherent heterogeneity of granular material, the estimation of thermal conduction involves simplified assumption of volumetric fraction of constituents and their

thermal properties, while thermal inertia and microstructure need to be under consideration [6]. Yet, this observation does not entail the fluid flow in granular materials.

Steady-state fluid flow is an important heat transport process in granular materials. Its effectiveness depends on the thermal properties of the material that makes the grains, the packing density of the granular bed, the fluid composition and the fluid velocity. Common industrial applications include heat and mass transfer operations, such as in chemical reactors [7–9]. Fluid-mediated heat transport must be considered in the analysis of geotechnical systems such enhanced geothermal recovery, borehole instability in deep wells, and ground response in nuclear waste disposal [10–12].

Can heat transfer take place in cyclic fluid flow through a granular medium of constant fabric? Cyclic fluid flow conditions arise at all scales and in a wide range of natural systems and engineering applications, from squirt-flow at intergranular contacts during cyclic loading, to large-scale oscillating flow in near-shore sediments driven by tidal motion. It is now well known that mass transport takes place during cyclic fluid flow; in fact, flow in-and-out of bones during physical exercise sustains bone development [13–15]. Yet, while heat transfer during cyclic fluid flow in granular materials has been used to evaluate thermal properties [16–18], the efficiency of heat transport during cyclic fluid flow in granular matter at constant fabric requires further understanding. Note that heat transfer in fluidized beds is reported in [8,16,19]. The amplitude of thermal energy in the open system (inlet $\neq$ outlet) keep decreasing as the heat is exchanged during cyclic temperature variation. On the other hand, there is no continuous flow of cyclic heat in the closed systems (inlet = outlet), where the heat is propagated by 'inter-phase heat exchange' between invading fluid and solid materials. This case resembles enhanced chemical diffusion [15]. Also note that heat exchanges and internal particle heat conduction in fluidized condition have been investigated [20,21].

The purpose of this study is to explore heat transfer in granular materials subjected to cyclic fluid flow in the closed system. Experiments and numerical simulations are designed to identify governing scales and the parameter space for optimal process performance. Particle level and packing-level studies follow.

2 Single particle: response to thermal step

The externally imposed time scale in cyclic flow is the cycle period t_{cy}. On the other hand, the characteristic time for particle-fluid heat transfer t_{ch} is the internal time scale for the process. Analogous to other physical processes, we anticipate that the ratio t_{cy}/t_{ch} will define different heat-transfer regimes in cyclic flow. The purpose of this first study is to determine the characteristic time t_{ch}.

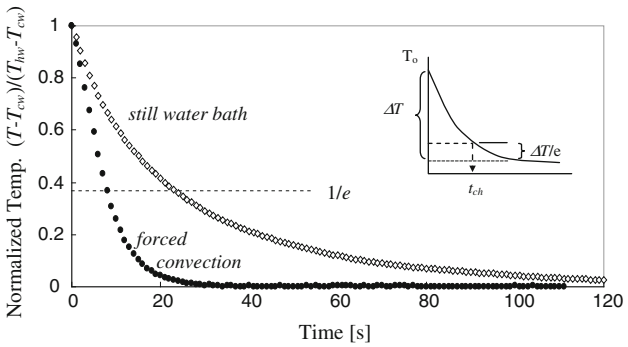

Fig. 1 Temperature change in a particle ($r_p = 0.0127$ m) when it is suddenly submerged in a large cold water bath. The insert shows the definition of the characteristic time t_{ch}. Data shown for cooling in still water and in stirred water

Experiment

An aluminum-bronze spherical particle (Alloy 630; radius $r_p = 12.7$ mm, thermal conductivity $k_p = 39.1\,\mathrm{W\,m^{-1}\,°C^{-1}}$, heat capacity $c_p = 0.38\,\mathrm{kJ\,kg^{-1}\,°C^{-1}}$, density $\rho_p = 7584\,\mathrm{kg\,m^{-3}}$) is instrumented with a 1 mm diameter thermocouple housed at its core. The particle is submerged in a hot water bath at constant temperature $T_{hw} = 49.5$°C. Once the equilibrium temperature is reached, the particle is quenched in a large-volume bath filled with cold water $T_{cw} = 20$°C. The evolution of the particle temperature in time $T_p(t)$ is monitored every 1 s. Figure 1 shows the temperature response during quenching for two test conditions, one in a still water bath and the other under forced convection by stirring.

Analysis

Conservation requires that the change of thermal energy in the particle per unit of time dQ/dt is equal to the heat transfer rate into the surrounding water $q(t)$ (W), i.e., $dQ/dt = q(t)$. The thermal energy in the particle is proportional to its volume, the specific heat c_p and mass density ρ_p of the material that makes the particle, and the particle temperature T_p. Let's assume that the interior temperature of the particle remains approximately uniform at all times, i.e., the time for internal thermal homogenization is much smaller than the time required for the particle to reach the bath temperature. Then,

$$\frac{dQ}{dt} = \frac{4}{3}\pi r_p^3 \rho_p c_p \frac{d\left[T_p\,(t)\right]}{dt} \tag{1}$$

The rate of heat transfer from the particle to the surrounding water $q(t)$ is proportional to the particle-water interfacial area $A_p\,(\mathrm{m}^2)$ and the temperature difference between the water T_w and the particle $T_p(t)$

$$q(t) = hA_p\left[T_w - T_p\,(t)\right] \tag{2}$$

where the particle-fluid heat transfer coefficient $h(\mathrm{W\,m^{-2}\,^{\circ}C^{-1}})$ captures interfacial conditions, and all types of heat transfer within the fluid for the given test conditions, i.e., convection, forced convection, and/or diffusion. Then, the particle temperature evolution in time is

$$\frac{d\left[T_p\,(t)\right]}{dt} = \frac{3}{4\pi}\frac{hA_p}{\rho_p c_p r_p^3}\left[T_w - T_p\,(t)\right] \tag{3}$$

Integrating from time $t = 0$-to-t and the initial particle temperature T_{pi} to $T_p(t)$ yields

$$\frac{T_p(t) - T_w}{T_{pi} - T_w} = \mathrm{e}^{\left(-\frac{3h}{\rho_p c_p r_p}t\right)} \tag{4}$$

Let's define the "characteristic time" t_{ch} as the time lapsed when the difference between the particle temperature and the medium $T_p(t) - T_w$ reduces to $1/e$ of the initial thermal difference $T_{pi} - T_w$. Setting Eq. 4 equal to $1/e$ results in

$$t_{ch} = \frac{\rho_p c_p r_p}{3h} \tag{5}$$

The characteristic time for the data shown in Fig. 1 is $t_{ch} = 23$ s for still water conditions and $t_{ch} = 8$ s for forced convection. The corresponding values for the heat transfer coefficient h computed from Eq. 5 are $h = 530\,\mathrm{W\,m^{-2}\,^{\circ}C^{-1}}$ for still water and $h = 1525\,\mathrm{W\,m^{-2}\,^{\circ}C^{-1}}$ for forced convection. These results show the predominance of convective heat flow on the rate of heat exchange between two materials.

The assumption made earlier that the time for internal thermal homogenization within the particle is much smaller than the time required for the particle to reach the bath temperature is satisfied when Biot's number is small

$$Biot = \frac{r_p h}{3k_p} < 0.1 \tag{6}$$

For these data $Biot = 0.06$ in still water, and the lumped mass model for negligible internal resistance assumed in Eq. 1 is adequate to capture the physical process.

3 Single particle: cyclic heat exchange

The successive immersion of a particle in a cold and a hot water baths is a form of mechanically-mediated heat transfer between two chambers. Such grain-fluid cyclic heat exchange is tested in this second study using the same aluminum-bronze particle as in the previous experiment.

Experiment

A large mass of hot water is kept at constant temperature $T_{hw} = 52^{\circ}$C in bath "A" (Fig. 2). The second bath "B" has a constant water mass of 100 g and starts at an initial temperature of $T_{cw} = 21^{\circ}$C. The particle is sequentially submerged

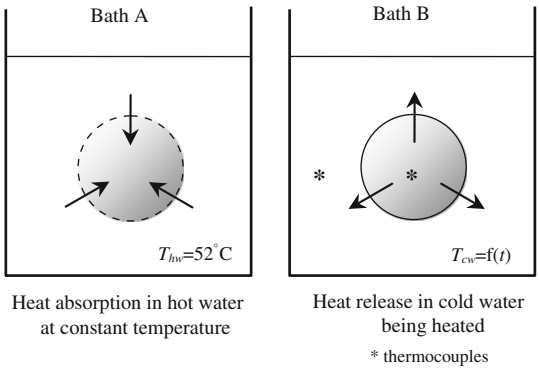

Fig. 2 Heat transfer by repeatedly moving a heated particle from the constant temperature hot water bath "A" into a cold water bath "B" of finite mass

in each bath with a pre-selected fixed periodicity t_{in} until the temperature of the cold water bath T_{cw} approaches an asymptote value.

The evolution of the particle temperature T_p (thermocouple housed at the core of the particle) and the temperature of the cold water bath T_{cw} are plotted in Fig. 3. Data are presented for cycle periods $t_{cy} = 100$ s and 200 s so that the total duration of the two tests is the same. The particle temperature oscillates as it absorbs and releases heat in each cycle. The bath B temperature T_{cw} increases when the heated particle is immersed in it, and it remains relatively constant while the particle is being heated in the constant temperature hot water bath A. At the end of the 5000 s total test duration, the temperature in Bath B reaches 45.2°C when $t_{cy} = 100$ s (50 cycles), and 42°C when $t_{cy} = 200$ s (25 cycles). Note that the immersion time in both studies, $t_{cy}/2 = 50$ s and 100 s, exceeds the characteristic time measured for this spherical particle, $t_{ch} = 23$ s. Therefore, there is sufficient time in each immersion to transfer most of the stored heat. Indeed, trends gathered in the two tests superimpose when the data are plotted versus the number of cycles (Fig. 3c).

Analysis

The rate of heat transfer and heat balance expressions (Eqs. 1, 2) can be written in finite difference form as follows

$$q^i = hA_p\left(T_p^i - T_{cw}^i\right)$$

heat transfer rate at time t_i- from Eq. 2 (7)

$$T_p^{i+1} = T_p^i - \frac{\Delta t}{\frac{4}{3}\pi r^3 \rho_p c_p} q^i$$

particle temperature at time t_{i+1}- from Eq. 1 (8)

$$T_{cw}^{i+1} = T_{cw}^i + \frac{\Delta t}{\rho_w c_w V_{bathB}} q^i$$

water temperature at time t_{i+1}- analogous to Eq. 1 (9)

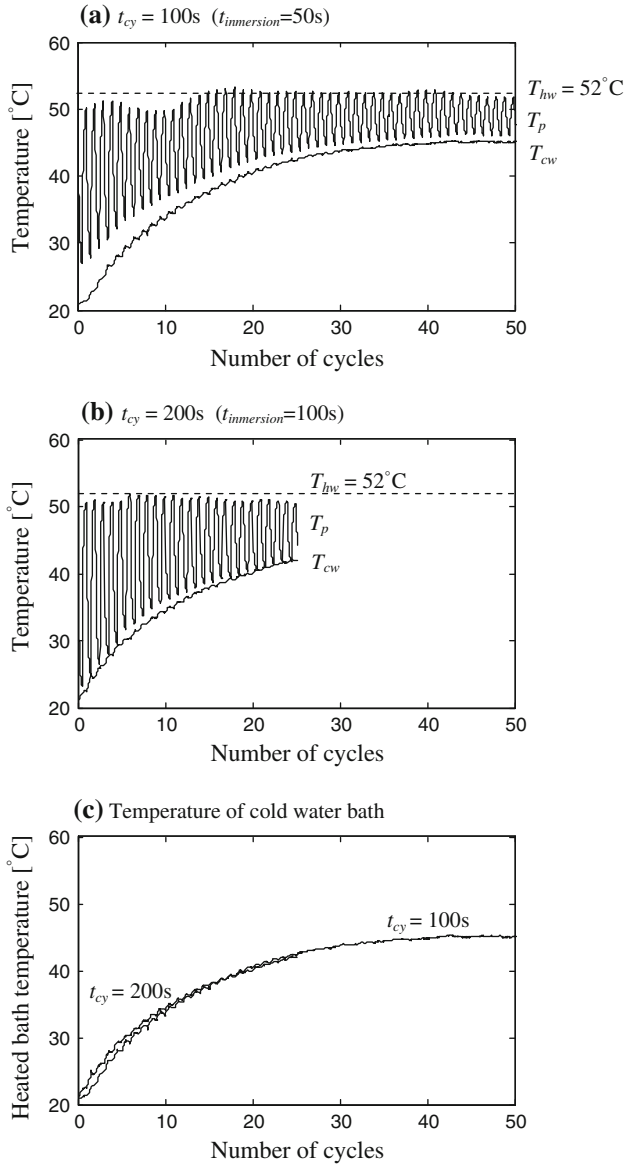

Fig. 3 Measured heat transfer in two-baths experiments. Temperature evolution with number of cycles for immersion duration $t_{cy} = 100$ s and 200 s. T_p: particle temperature. T_{hw}: constant hot water bath temperature 52°C.T_{cw}: cold water bath temperature

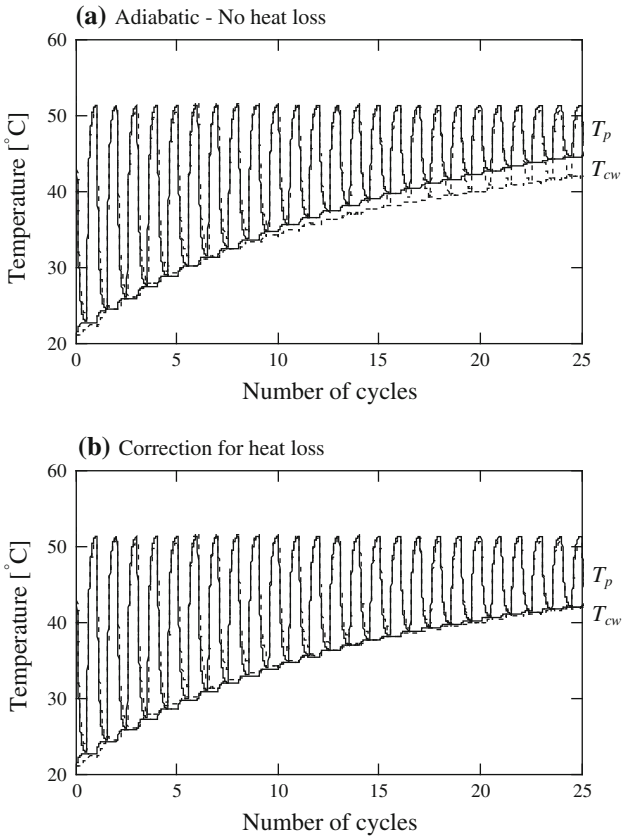

Fig. 4 Experimental data (*dotted lines*) and numerical prediction (*solid lines*) corresponding to the particle and the water bath temperature evolution—Cycle duration $t_{cy} = 200$ s. Numerical predictions in each frame assume: **a** adiabatic conditions—the overestimated bath temperature increases with time; and **b** heat loss to the surroundings (fitting value: $\Psi = 0.05\text{W}\,^\circ\text{C}^{-1}$). Note: T_p particle temperature; T_{cw} cold water bath temperature

where V_{bathB} is the volume of water in the cold water bath B. These expressions permit computing the evolution of the particle and water bath temperatures at time $t_{i+1} = t_i + \Delta t$ as a function of the temperatures at time t_i where Δt is the time increment.

Figure 4a shows measured and predicted temperatures when the cycle duration is $t_{cy} = 200$ s. Predicted values are numerically computed every $\Delta t = 1$ s using a heat transfer coefficient $h = 530\text{W m}^{-2}\,^\circ\text{C}^{-1}$ (without forced convection—Fig. 1). The measured exponential cooling and heating of the particle are well captured in the simulation. The temperature of the water Bath B is overestimated in Fig. 4a, suggesting heat loss into the surroundings. A heat loss term proportional to the temperature difference between the cold water bath T_{cw} and the room temperature T_{room} is introduced in Eq. 7,

$$q^i = hA_p(T_p^i - T_{cw}^i) - \Psi(T_{cw}^i - T_{room}) \tag{10}$$

where $\Psi(\text{W}\,^\circ\text{C}^{-1})$ is the heat loss coefficient. The corrected temperature evolution is plotted in Fig. 4b for a heat loss coefficient $\Psi = 0.05\text{W}\,^\circ\text{C}^{-1}$ that is determined by fitting experimental data with numerically computed values.

The number of cycles is inversely proportional to the immersion time for a given test duration t_t. Therefore, longer immersion times allow for more thorough particle-water heat exchange while shorter immersion times permit a larger number of cycles per unit of time but at a diminished heat exchange per cycle. Hence, we anticipate a trade-off between immersion time and the number of cycles, and the emergence of an optimal test condition for maximum time-average heat transfer. The finite difference algorithm described above

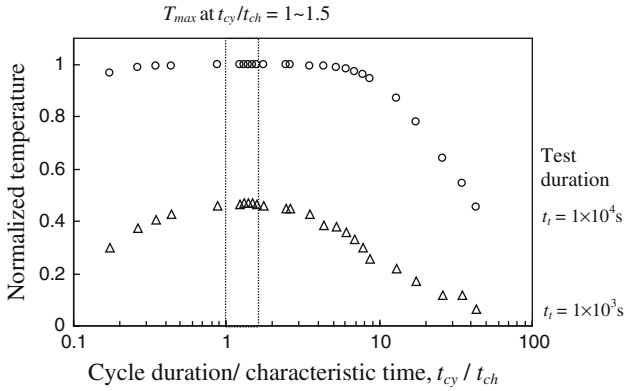

Fig. 5 Predicted temperature of the water bath at selected times for different cycle durations t_{cy}. The maximum temperature is obtained when t_{cy}/t_{ch} is $1 \sim 1.5$, where the characteristic time $t_{ch} = 23$ s. The normalized temperature in y-axis represents $(T_{predicted} - T_{cw})/(T_{hw} - T_{cw})$

is used to explore the different process regimes, in terms of the ratio between the cycle period and the characteristic time t_{cy}/t_{ch}, using material parameters and conditions corresponding to the tests reported in Fig. 3. Results are shown in Fig. 5 for both short and long duration tests ($t_t = 1 \times 10^3$ s and 1×10^4 s with constant characteristic time $t_{ch} = 23$ s in Fig. 1). Time and temperature are presented in dimensionless form to facilitate the comparison of test results. The normalized temperature in the y-axis, $(T_{predicted} - T_{cw})/(T_{hw} - T_{cw})$ captures the evolution of the medium temperature during cyclic heating between the two extreme system temperatures T_{hw} and T_{cw}. Due to the short test duration and losses, the bath temperature reaches only $(T_{predicted} - T_{cw})/(T_{hw} - T_{cw}) \sim 0.4$. The optimal operating regime is better defined in short-duration tests: $t_{cy}/t_{ch} = 1 \sim 1.5$ for a test duration $t_t = 1 \times 10^3$ s. The benefit of operating in the optimal t_{cy}/t_{ch} window diminishes for longer duration tests.

4 Granular medium: heat transport during cyclic fluid flow

Granular beds hinder particle movement so heat transport can not be based on cyclic grain displacement, as in the previous section. Instead, we explore herein the case of heat transport driven by cyclic fluid flow in the granular bed. The anticipated sequence of events for the case of a granular medium with a pervious boundary against a constant hot fluid reservoir follows (Fig. 6a):

- first invasion phase: hot fluid from the reservoir moves up and invades the granular medium to a certain distance $x = \Delta L$ and heat is transferred to the particles,
- first drainage phase: the colder saturating fluid at a distance $x > \Delta L$ moves down towards the boundary and picks up heat from the grains,
- second invasion phase: the hotter saturating fluids in the zone $0 \le x \le \Delta L$ moves up and transports heat further into the granular bed to a distance $x \le 2\Delta L$.

This mental experiment shows heat transport in granular materials driven by cyclic fluid flow. We investigate this phenomenon using both experimental and numerical methods next.

Experiment

The specimen consists of water-saturated quartz sand (Ottawa sand; $D_{50} = 0.72$ mm, $C_u = 1.15$, porosity $n = 0.4$) packed inside a Plexiglas cylinder (diameter = 70 mm, height = 400 mm). Fifteen thermocouples are embedded every 20 mm along the specimen height to monitor temperature (1 s sampling interval—Fig. 7). Cyclic fluid flow is enforced through the bottom port using a three-way valve. Hot water is introduced to a height $\Delta L = 20$ mm (~30 particles diameter), then, the same volume of water is drained out of the sand. Invasion and drainage stages last ~5 s and are much shorter than the complete cycle to minimize heat exchange during fluid flow (Fig. 6b). The water surface remains above the sediment surface at all times. The initial temperature of the saturated sand column for the various tests is 30-to-32°C and the temperature of the hot water reservoir is 50-to-55°C.

Figure 8 shows the temperature evolution with time at different heights away from the entry port for three cycle periods $t_{cy} = 20$ s, 60 s and 120 s. The data clearly show heat transport along the column prompted by the cyclic fluid flow. Temperature oscillations reflect each flow cycle; tests with longer cycle t_{cy} show slower temperature evolution. Measurements at different elevations do not seem to converge to a single temperature; this implies heat loss from the column into the surrounding medium.

Analysis

Let's assume that all heat transport in the column results from cyclic fluid flow as described in the mind-experiment above, so that there would be no heat transport in the absence of fluid flow. The column is discretized into segments of length equal to the invasion distance ΔL in Fig. 6c. The fluid in segment $i-1$ at temperature T_{i-1} invades the ith segment and remains there until the temperature reaches equilibrium (i.e., "long cycle" regime). At thermal equilibrium,

$$q_{fluid} - q_{paricle} = c_w m_w (T_w - T_i) - c_s m_s (T_i - T_s) \quad (11)$$

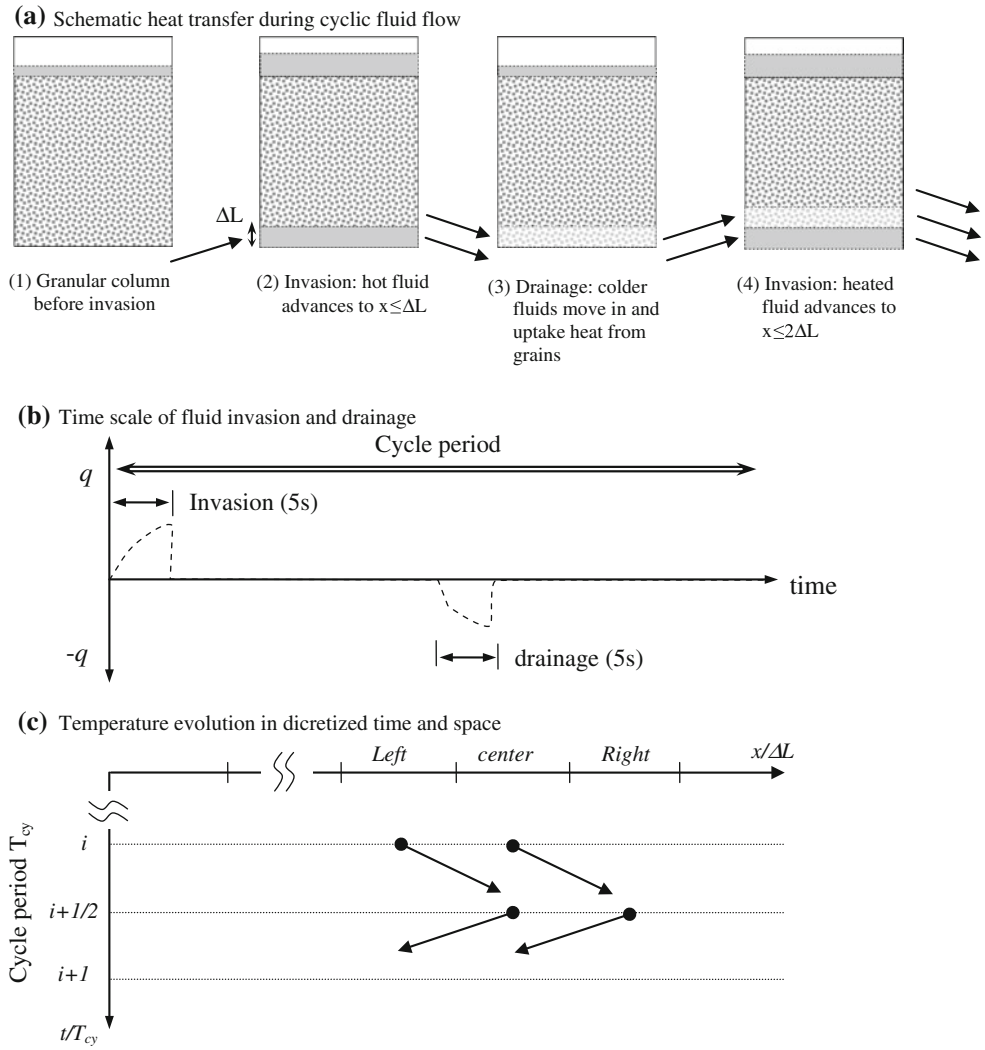

Fig. 6 **a** Heat transport during cyclic fluid flow. **a-1** A granular column sits on a hot fluid reservoir. **a-2** Hot fluid invades the sediment to height x $\leq$ ΔL and transfers heat to grains. **a-3** During the partial drainage phase, colder fluids further away from the boundary x $>$ ΔL move down and uptake heat stored in the granular medium. **a-4** The new invasion cycle moves the warmer fluids further up to x $\leq 2\Delta$L. **b** Duration of invasion and drainage phases compared to cycle duration. **c** Tracking temperature evolution in discrete time and space

Then, the temperature in the ith segment in the middle of the jth cycle is (Note: a full cycle consists of both fluid invasion and discharge)

$$T_i^{j+\frac{1}{2}} = \frac{T_{i-1}^j (m_w c_w) + T_i^j (m_p c_p)}{m_w c_w + m_p c_p} = \alpha T_{i-1}^j + (1-\alpha)\, T_i^j \tag{12}$$

where α is a function of the mass m and specific heat c of water and particles. The coefficient α can be then expressed as a function of the water content in the granular medium $w$which is the ratio of mass of water to mass of particles, $w = m_w/m_p$,

$$\alpha = \frac{m_w c_w}{m_w c_w + m_p c_p} = \frac{w}{w + \frac{c_p}{c_w}} \tag{13}$$

At the same time, the temperature T_{i+1} for the adjacent segment $i+1$ is

$$T_{i+1}^{j+\frac{1}{2}} = \frac{T_{i+1}^j (m_p c_p) + T_i^j (m_w c_w)}{m_w c_w + m_p c_p} = \alpha T_i^j + (1-\alpha)\, T_{i+1}^j \tag{14}$$

During the discharge phase of the cycle, the fluid that occupied the $i+1$ segment at the end of the invasion phase $(j+1/2)$ returns to the ith segment. Then, the temperature in the ith segment at the end of the cycle is obtained by combining Eqs. 12 and 14

$$\begin{aligned} T_i^{j+1} &= \alpha T_{i+1}^{j+\frac{1}{2}} + (1-\alpha)\, T_i^{j+\frac{1}{2}} \\ &= \alpha\,(1-\alpha)\left(T_{i-1}^j + T_{i+1}^j\right) + \left[\alpha^2 + (1-\alpha)^2\right] T_i^j \end{aligned} \tag{15}$$

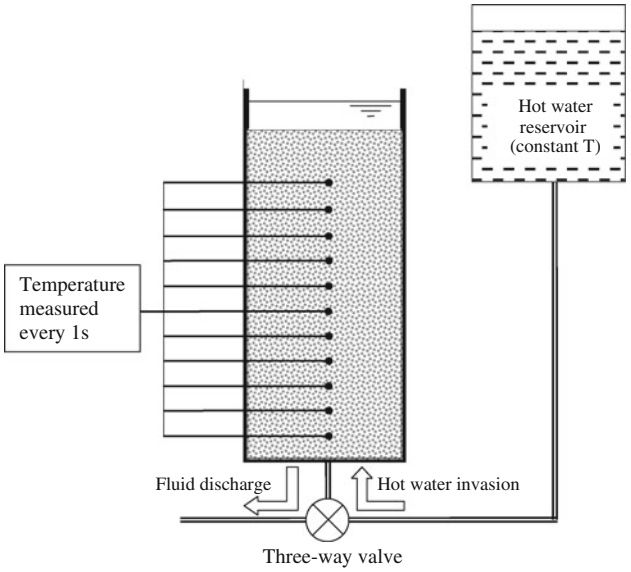

Fig. 7 Experimental configuration used to study heat transfer during cyclic fluid flow in a granular medium

In Fig. 8, we superimpose the numerically predicted temperature trends at the end of each cycle over the cyclic response measured in the tests. A heat loss term, $\lambda(T_i^j - T_{room})$ equivalent to Eq. 10, is included to capture the lower asymptotic temperature values at higher elevations away from the entry port.

5 Discussion

The one-dimensional thermal diffusion equation relates temporal and spatial changes in temperature through the thermal diffusion coefficient $D(\mathrm{m^2\,s^{-1}})$

$$\frac{\partial T}{\partial t} = D\frac{\partial^2 T}{\partial x^2} \tag{16}$$

The first order finite difference approximation is

$$T_i^{j+1} = M(T_{i-1}^j + T_{i+1}^j) + (1-2M)T_i^j \tag{17}$$

where the modulus is $M = D \cdot t/\Delta x^2$ and Δt and Δx indicate the discretization of time and space. Eqs. 15 and 17 are equivalent when $M = \alpha - \alpha^2$, assuming the equilibrium restriction applies (Eq. 6), i.e., trends predicted using Eqs. 15 and 17 are identical on Fig. 8. In other words, heat transfer in cyclic fluid flow is equivalent to thermal diffusion with diffusivity D_{cy}

$$D_{cy} = \frac{\Delta L^2}{t_{cy}} \frac{\frac{c_s}{c_w} w}{\left(\frac{c_s}{c_w} + w\right)^2} \tag{18}$$

Thus, the equivalent thermal diffusivity is determined by the cyclic flow parameters, invasion height ΔL and cycle

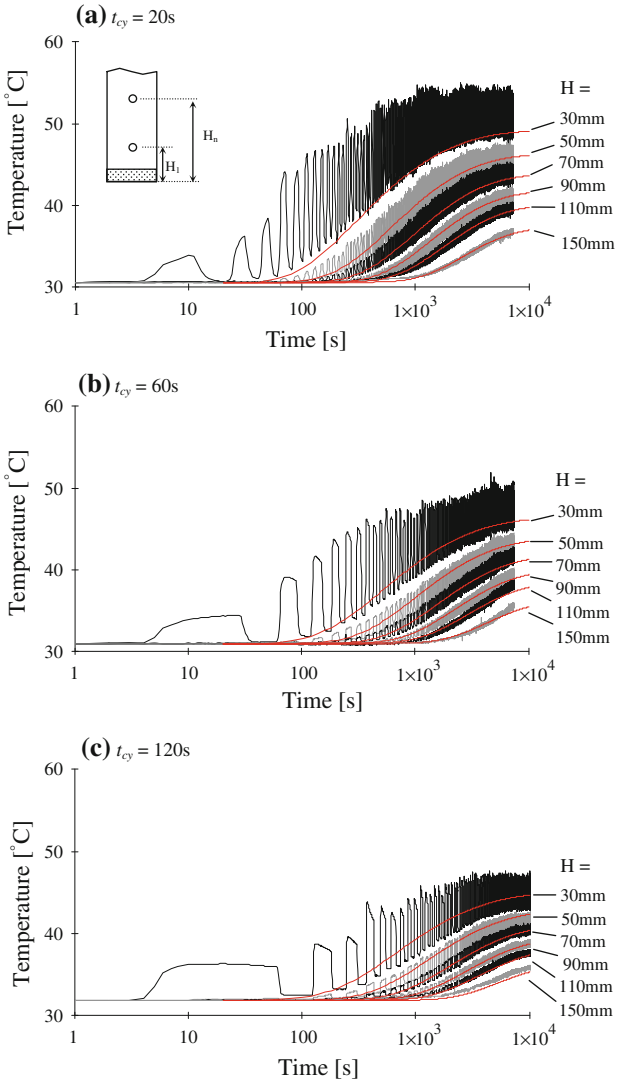

Fig. 8 Temperature evolution during cyclic fluid flow. Experimentally measured temperature evolution at different distances away from the entry port for three cycle periods **a** $t_{cy} = 20\,\mathrm{s}$, **b** $t_{cy} = 60\,\mathrm{s}$ and **c** $t_{cy} = 120\,\mathrm{s}$. The smooth lines (non-oscillating) lines are the numerically predicted temperature at the end of each cycle using either the cyclic fluid flow formulation (Eq. 15) or the equivalent diffusion Eq. 18. Note: both expressions are modified to take into consideration heat loss along the column

duration t_{cy}. The second factor in Eq. 18 depends on material parameters and is typically ≤ 0.2 for water saturated geological sediments; more advantageous heat transport conditions may be attained in other grain-fluid systems. It is worthwhile noting that analogous mass exchange-and-transport develops in cyclic fluid flow and it manifests as an equivalent diffusion-type response at the macro-scale as well (see details in [15]).

We assumed no thermal diffusion in our cyclic fluid flow analysis. However, diffusive transport in cyclic fluid flow combines thermal diffusion under hydrostatic conditions D

Table 1 Measured and estimated parameters

Cycle period t_{cy} (s)	Fitted diffusion Eq.		Computed diffusivity in cyclic fluid flow D_{cy} ($m^2\ s^{-1}$)	Diffusion no fluid flow D($m^2\ s^{-1}$)
	Diffusivity D_{eff}($m^2\ s^{-1}$)	Heat loss λ(s^{-1})		
20	2.5×10^{-6}	0.00046	3.46×10^{-6}	measured: 0.8×10^{-6}bounds*: $0.3 \times 10^{-6} \leq D \leq 1.3 \times 10^{-6}$
60	1.5×10^{-6}	0.003	1.15×10^{-6}	
120	1.2×10^{-6}	0.0025	5.77×10^{-7}	

* Parallel and series bounds

with diffusion in cyclic flow D_{cy} to produce the effective diffusion D_{eff}

$$D_{eff} = D + D_{cy} \tag{19}$$

The values of diffusivity identified by matching experimental results in Fig. 8 correspond to D_{eff}. Table 1 presents a summary of fitted values D_{eff} and computed values D_{cy} (Eq. 18). For comparison, the measured thermal diffusion coefficient without fluid flow is presented in the table. Both measured and predicted thermal diffusivity values D_{eff} and D_{cy} clearly decrease with increasing cyclic period t_{cy}.

The characteristic time for sand particles $t_{ch} \sim 0.2$ s is estimated using the empirical correlation between Peclet and Nusselt numbers for a fluidized bed in [19]. Note that the estimated grain characteristic time is shorter than the invasion-drainage phases and the cyclic periods used in the tests. Therefore, extensive heat exchange takes place while water flows in and out of the granular bed; this explains the lower sensitivity to t_{cy} than theoretically predicted (Table 1). Given that $t_{ch} \ll t_{cy}$, shorter cycle periods could be applied to increase the effective heat transport per unit of time.

The heat loss coefficient Ψ is simultaneously determined while fitting numerical predictions to experimental results (Table 1). Heat loss is proportional to the difference between the surrounding temperature and the temperature inside the cell. Therefore, heat loss increases during the test and is inversely proportional to the effective thermal diffusivity of the medium. Note that the available expressions for heat transfer in packed beds apply to steady flow rather than the cyclic fluid flow [22]. The steady flow velocity or time-average velocity in this study is zero. Therefore, reported correlations predict a null heat transfer coefficient. Instead, upper and lower bounds for heat diffusion in packed beds are compared with measured values (Table 1).

An incompressible one-dimensional system experiences the same flow rate along the body. This is not the case in compressible systems where the flow rate decreases away from the pervious boundary; the efficiency of heat transport should decrease accordingly. High invasion length in short time requires high gradients, which may eventually cause hydro-mechanical effects including instabilities within the granular medium.

6 Conclusions

Heat transport in granular media subjected to cyclic fluid flow under constant fabric can be a significant transport process.

Mathematically, heat transport in cyclic fluid flow is equivalent to diffusion, where the effective diffusivity is proportional to the square of the invasion depth and inversely proportional to the cycle period.

Heat transport during cyclic fluid flow is restricted by the characteristic internal time for fluid-grain heat transfer t_{ch}. Optimal transfer conditions develop when $t_{cy}/t_{ch} = 1 \sim 1.5$.

Anticipated implications of heat transport during cyclic fluid flow extend to natural systems (daily tidal fluctuation, hydrothermal chimneys in the seafloor), engineered cooling (from microelectronics to buildings and pavements), and biomedical applications (tissue recovery and preservation).

Acknowledgments Support for this research was provided by P.C. Rossin College of Engineering and Applied Science at Lehigh University, Yonsei University Research Fund of 2009 (No.2009-1-0193) and both the Goizueta Foundation and JIP-Chevron project at Georgia Institute of Technology.

References

1. Weidenfeld, G., Weiss, Y., Kalman, H.: A theoretical model for effective thermal conductivity (ETC) of particulate beds under compression. Granul. Matter **6**(2–3), 121–129 (2004)
2. Cote, J., Konrad, J.-M.: A generalized thermal conductivity model for soils and construction materials. Can. Geotech. J. **42**(2), 443–458 (2005)

3. Yun, T.S., Santamarina, J.C.: Fundamental study of thermal conduction in dry soils. Granul. Matter **10**(3), 197–207 (2008)
4. Mizonov, V., Berthiaux, H., Arlabosse, P., Djerroud, D.: Application of the theory of Markov chains to model heat and mass transfer between stochastically moving particulate and gas flows. Granul. Matter **10**(4), 335–340 (2008)
5. Batchelor, G.K., O'Brien, R.W.: Thermal or electrical conduction through a granular material. Proc. Roy. Soc. Lond. Ser. A: Math. Phys. Sci. **355**(1682), 313–333 (1977)
6. Ordonez-Miranda, J., Alvarado-Gil, J.J.: Thermal characterization of granular materials using a thermal-wave resonant cavity under the dual-phase lag model of heat conduction. Granul. Matter (2010, in print)
7. Dwivedi, P.N., Upadhyay, S.N.: Particle-fluid mass transfer in fixed and fluidized beds. Ind. Eng. Chem. Process Des. Dev. **16**(2), 157–165 (1977)
8. Gupta, S.N., Chaube, R.B., Upadhyay, S.N.: Fluid-particle heat transfer in fixed and fluidized beds. Chem. Eng. Sci. **29**(3), 839–843 (1974)
9. Gillespie, B.M., Crandall, E.D., Carberry, J.J.: Local and average interphase heat transfer coefficients in a randomly packed bed of spheres. AIChE J. **14**(3), 483–490 (1968)
10. Olivella, S., Carrera, J., Gens, A., Alonso, E.E.: Nonisothermal multiphase flow of brine and gas through saline media. Transp. Porous Media **15**(3), 271–293 (1994)
11. Gens, A., Garcia-Molina, A.J., Olivella, S., Alonso, E.E., Huertas, F.: Analysis of a full scale in situ test simulating repository conditions. Int. J. Num. Anal. Methods Geomech. **22**(7), 515–548 (1998)
12. Wang, Y., Dusseault, M.B.: A coupled conductive-convective thermo-poroelastic solution and implications for wellbore stability. J. Petrol. Sci. Eng. **38**(3–4), 187–198 (2003)
13. Piekarski, K., Munro, M.: Transport mechanism operating between blood supply and osteocytes in long bones. Nature **269**, 80–82 (1977)
14. Wang, L., Cowin, S.C., Weinbaum, S., Fritton, S.P.: Modeling tracer transport in an Osteon under cyclic loading. Ann. Biomed. Eng. **28**, 1200–1209 (2000)
15. Goldsztein, G.H., Santamarina, J.C.: Solute transport during cyclic flow in saturated porous media. Appl. Phys. Lett. **85**(12), 2432–2434 (2004)
16. Lindauer, G.C.: Heat transfer in packed and fluidized beds by the method of cyclic temperature variations. AIChE J. **13**(6), 1181–1187 (1967)
17. Goss, M.J., Turner, G.A.: Simultaneous computation of heat transfer and dispersion coefficients and thermal conductivity value in a packed bed of spheres: III. Experimental method and results. AIChE J. **17**(3), 592–595 (1971)
18. Gunn, D.J., De Souza, J.F.C.: Heat tranfer and axial dispersion in packed beds. Chem. Eng. Sci. **29**, 1363–1371 (1974)
19. Al-zahrani, A.A., Al-tajam, M.: Measurement of heat transfer coefficient for liquid-solid fluidized beds. Powder Technol. **80**, 25–28 (1994)
20. Haim, M., Kalman, H.: The effect of internal particle heat conduction on heat transfer analysis of turbulent gas-particle flow in a dilute state. Granul. Matter **10**(4), 341–349 (2008)
21. Biggs, M.J., Glass, D., Xie, L.: Granular temperature in a gas fluidized bed. Granul. Matter **10**(2), 63–73 (2008)
22. Seshadri, V., Silva Pereira, R.O.: Comparison of formulae for determining heat transfer coefficient of packed beds. Trans. Iron Steel Inst. Japan **26**(7), 604–610 (1986)